

## The Structural Basis of the TIM10 Chaperone Assembly\*

Received for publication, December 1, 2003, and in revised form, January 20, 2004  
Published, JBC Papers in Press, February 18, 2004, DOI 10.1074/jbc.M313046200

Hui Lu‡, Alexander P. Golovanov§, Felicity Alcock‡, J. Günter Grossmann¶, Scott Allen‡, Lu-Yun Lian§, and Kostas Tokatlidis‡¶\*\*

From the ‡School of Biological Sciences, University of Manchester, Oxford Road, Manchester M13 9PT, United Kingdom, §Department of Biomolecular Sciences, Jackson Mill, University of Manchester Institute of Science and Technology, Manchester M60 1QD, United Kingdom, ¶Council for the Central Laboratory of the Research Councils, Daresbury Laboratory, Synchrotron Radiation Department, Warrington, Cheshire WA4 4AD, United Kingdom, and ||Department of Chemistry, University of Crete, P. O. Box 1470, 714 09 Heraklion and Institute of Molecular Biology and Biotechnology-Foundation for Research and Technology (IMBB-FORTH), P. O. Box 1527, 711 10 Heraklion, Greece

**Tim9 and Tim10 are essential components of the “small Tim” family of proteins that facilitate insertion of polytopic proteins at the inner mitochondrial membrane. The small Tims are themselves imported from the cytosol and are organized in specific translocation assemblies in the intermembrane space. Their conformational properties and how these influence the mechanism of assembly remain poorly understood. Moreover, the three-dimensional structure of the TIM10 complex is unknown. We have characterized the structural properties of these proteins in their free and assembled states using NMR, circular dichroism, and small angle x-ray scattering. We show that the free proteins are largely unfolded in their reduced assembly-incompetent state and molten globules in their oxidized assembly-competent state. Tim10 appears less structured than Tim9 in their respective free oxidized forms and undergoes a larger structural change than Tim9 upon complexation. The NMR data here demonstrates unequivocally that only the oxidized states of the Tim9 and Tim10 proteins are capable of forming a complex. Zinc binding stabilizes the reduced state against proteolysis without significantly affecting the secondary structure. Solution x-ray scattering was used to obtain a molecular envelope for the subunits individually and for their fully functional TIM10 complex. *Ab initio* shape reconstructions based on the scattering data has allowed us to obtain the first low resolution three-dimensional structure of the TIM10 complex. This is a novel structure that displays extensive surface hydrophobicity. The structure also provides an explanation for the escorting function of this non-ATP-powered chaperone particle.**

A universal event for the successful construction and function of all of the cells is that proteins are targeted to their correct location both spatially and temporally. The extent of these targeting events is reflected by the fact that more than one-third of the proteome of the cell are translocated across or inserted into a membrane. Mitochondria represent a major site for extensive protein translocation. Virtually all of the mito-

chondrial proteins (approximately one thousand different polypeptides) are imported from the cytosol and are sorted within the organelle. This event is orchestrated by distinct translocation machineries in the outer (translocase of the outer membrane, TOM)<sup>1</sup> and inner (translocase of the inner membrane, TIM) membranes and within the intermembrane space. An intriguing new class of translocase proteins is the small Tim family, which specifically mediates the import of presequence-devoid polytopic proteins.

There are two main pathways for proteins destined to mitochondria. The matrix pathway is used mainly by precursors that contain a cleavable presequence (1), whereas precursors devoid of a presequence divert through the distinct carrier pathway (2–5). The small Tims are organized in two distinct 70-kDa complexes in the intermembrane space, the TIM10 complex that is made of Tim9 and Tim10, which are encoded by essential genes in yeast (6–9), and the Tim8/13 complex made of Tim8 and Tim13, which are encoded by genes dispensable in yeast (10–12). The two complexes operate in the carrier pathway with different substrate specificities but both in coordination with the essential insertion-specific TIM22 complex in the inner membrane (13). TIM10 is in large excess over Tim8 and Tim13 and over the TIM22 complex (3, 6), which also contains the homologous Tim12 protein (7, 8).

The TIM10 complex prevents aggregation of the hydrophobic substrate acting as a chaperone (2, 14). It binds to the transmembrane segments of the precursor as it emerges from the TOM channel (15, 16), facilitating in this way passage of these hydrophobic molecules across the aqueous environment of the intermembrane space (2–5). In contrast to most other chaperones, TIM10 does not require ATP hydrolysis and interacts specifically with membrane proteins. Although it has been shown that Tim9 and Tim10 are necessary and sufficient to form the complex (17), how the functional chaperone assembles is unclear. Similar to other small Tim proteins, Tim9 and Tim10 themselves must, in the first instance, be imported into the intermembrane space before they can fulfill their own specific roles in the transport of other mitochondrial proteins from the intermembrane space to the inner membrane. This process depends on the formation of the functional TIM10 complex. The structural basis for and the mechanism of this TIM10 assembly process, which includes import, folding, and subsequent com-

\* This work in our laboratory is funded by the Wellcome Trust (to K. T. and L.-Y. L.), the Medical Research Council (MRC), Biotechnology and Biological Sciences Research Council, and the Leverhulme Trust (to K. T.) and an MRC co-operative group grant (to K. T.). The costs of publication of this article were defrayed in part by the payment of page charges. This article must therefore be hereby marked “advertisement” in accordance with 18 U.S.C. Section 1734 solely to indicate this fact.

\*\* A Lister Institute Research Fellow. To whom correspondence should be addressed. Tel.: 30-2810-391136; Fax: 30-2810-391101; E-mail: tokatlid@imbb.forth.gr.

<sup>1</sup> The abbreviations used are: TOM, translocase of the outer membrane; TIM, translocase of the inner membrane; SAXS, solution x-ray scattering; ITC, isothermal titration calorimetry; DTT, dithiothreitol; Tricine, N-[2-hydroxy-1,1-bis(hydroxymethyl)ethyl]glycine; R<sub>g</sub>, radius of gyration; D<sub>max</sub>, maximum molecular dimension; ANS, 8-anilino-1-naphthalenesulfonic acid; HSQC, heteronuclear single quantum correlation; WT, wild type.

plexation for the individual subunits, and their regulation by redox state(s) remain unresolved.

A unique feature of the sequence of all small Tims is the strictly conserved "twin CX3C" motif separated from each other by 11–16 residues. Whether *in vivo* the cysteines are exclusively involved in ligation to zinc (similar to the zinc fingers) (18) or are disulfide-bridged (15, 19) is again unclear. Nevertheless, the significance of the cysteine residues, whatever are their precise roles, is partly borne out in mutagenesis studies of homologous proteins. Mutation of the fourth cysteine residue in DDP1 (the human homologue of Tim8) affects the folding of the Tim8 protein and Tim8-Tim13 assembly (20, 21). We have recently shown that the TIM10 complex is only formed between oxidized Tim 9 and Tim10 and that zinc can bind only to the fully reduced state without promoting complex formation (44). The combined data so far demonstrate the presence of an intimate relationship between, on one hand, the structure integrity, oxidation, and metal chelation states involving cysteine residues and, on the other, the formation of functional Tim9/Tim10 complexes. *In vivo*, the most stable form of the proteins is their complexed state. All of the other possible species (*i.e.* reduced apoprotein, reduced and bound to zinc but not assembled or oxidized but not yet assembled), are transient and short-lived. As a consequence, a study of the structural properties of these different states and how they underpin assembly is only possible *in vitro* using purified components.

Here we characterized the conformations of Tim9 and Tim10 under different redox and metal binding conditions. We present direct experimental evidence explaining the dependence on the redox state of these proteins for successful complex formation. The individual proteins are unfolded in the reduced state and adopt a partially folded molten-globule conformation upon oxidation. The "twin CX3C" motif is vital for the folding of the individual subunits through the formation of intramolecular disulfides, in agreement with previous mapping of the observed disulfides in Tim10 (19). The structural properties of the different states support reinforce the notion that the complex is made only from oxidized intramolecularly disulfide-bonded subunits, whereas intermolecular disulfides result in abortive misfolded species. Although zinc does not appear to play a direct role in complex formation, it stabilizes the reduced proteins against proteolysis. The complex remains flexible, although the NMR data showed that it is more structured than the oxidized individual subunits. We determined the low resolution three-dimensional structure of the individual subunits and of their complex by solution x-ray scattering (SAXS). The information from this finding provides new insights into the way TIM10 functions. The results here also suggest that TIM10 assembly is regulated by distinct structural states that correlate with the different redox state(s) of Tim9 and Tim10. In summary, there appears to be a hierarchy of "structures," with the reduced proteins having the least defined and the most flexible structures and the oxidized complex possessing the most pronounced structural features. This transformation of structures fits with the structural and energetic requirements for efficient protein transport and complex assembly.

#### EXPERIMENTAL PROCEDURES

**DNA Constructs and Proteins**—Tim9 and Tim10 WT or single Cys mutants were purified from *Escherichia coli* in a recombinant form as described previously (19). The recombinant TIM10 complex formation was performed as described previously (14).

**<sup>15</sup>N Labeling of Tim9 and Tim10**—*E. coli* strain BL21-Codonplus (Stratagene) containing a plasmid expressing glutathione *S*-transferase-Tim9 or glutathione *S*-transferase-Tim10 was grown in 50 ml of LB-AMP at 37 °C for 12–16 h. Cells were harvested at 5600 × *g* for 5 min at 4 °C and then resuspended in 5 ml of LB. A 2.5-ml cell suspension was added to 11 minimal medium (7 mM Na<sub>2</sub>HPO<sub>4</sub>, 55 mM KH<sub>2</sub>PO<sub>4</sub>,

22 mM glucose, 18.4 mM <sup>15</sup>NH<sub>4</sub>Cl, 1 mM MgSO<sub>4</sub>, 0.1 mM CaCl<sub>2</sub>, 100 mg/liter ampicillin, 30 μM thiamine-HCl), and growth continued at 37 °C until 0.7 > A<sub>600 nm</sub> > 0.9. Isopropyl-1-thio-β-D-galactopyranoside (0.1 mM) was then added to induce the expression of the fusion protein, and growth continued for ~4 h until 2.2 > A<sub>600 nm</sub> > 2.8. Cells were harvested by centrifugation (5600 × *g*, 4 °C, 15 min), washed with buffer A (50 mM Tris-HCl (pH 7.4), 150 mM NaCl) and resuspended in 25 ml of buffer A plus 0.1 mg/ml lysozyme. Cells were broken by sonication with a tapered microtip at 20% amplification for 3 min or by French press at 1000 p.s.i. The soluble part was isolated by centrifugation (21,000 × *g*, 4 °C, 30 min) and incubated overnight with glutathione-agarose beads (Sigma) equilibrated with buffer A. The non-bound proteins were collected, and beads were washed with 50 ml of buffer A. After washing, the beads were resuspended with 10 ml of buffer A containing 5 units/ml of thrombin (Sigma) and incubated overnight at 4 °C. The Tim10 protein was eluted with an additional 10 ml of buffer A. After disruption of induced cells by sonication or French press, the majority of the fusion protein was found in inclusion bodies (in the pellet). These were solubilized in denaturing buffer (150 mM NaCl, 50 mM Tris-HCl, 8 M urea (pH 8.0)) for 1 h at room temperature, separated from insoluble matter by centrifugation (21,000 × *g*, 20 °C, 30 min), and renatured overnight at 4 °C by a 10-fold dilution with buffer A. The renatured glutathione *S*-transferase fusion protein was separated from precipitated material by centrifugation at 21,000 × *g* for 15 min at 4 °C and then incubated with glutathione-agarose beads and further purified as described above.

**NMR Spectra**—One-dimensional <sup>1</sup>H NMR and two-dimensional <sup>1</sup>H-<sup>15</sup>N-heteronuclear single quantum correlation (HSQC) spectra were acquired at 293 K on Bruker DRX600 spectrometer. <sup>15</sup>N-filtered <sup>1</sup>H spectra were acquired at 318 K using one-dimensional version of <sup>1</sup>H-<sup>15</sup>N-HSQC pulse sequence. Free induction decay (acquisition time 0.128 s) was multiplied by square sine window function shifted by 72°, and zero-filled to 8192 points before Fourier transformation. Protein samples (concentration 0.2–0.3 mM) were dissolved in 50 mM phosphate buffer (pH 7.2) containing 150 mM NaCl and 90% H<sub>2</sub>O and 10% <sup>2</sup>H<sub>2</sub>O.

**Isothermal Titration Calorimetry**—Isothermal titration calorimetry for the binding of Zn<sup>2+</sup> to Tim9, Tim10, and mutants was performed in 10 mM of metal-free HEPES buffer (pH 7.6), 1 mM TCEP (Tris-[2-carboxyethyl]phosphine) at 30 °C with a VP-isothermal titration calorimetry (ITC) microcalorimeter. The metal-free buffer was prepared by incubation of 10 mM HEPES with Chelex-100 (Sigma) at 37 °C for 1 h to remove residual metals. Protein was dialyzed and reduced in the buffer containing 1 mM TCEP overnight. Protein then was loaded in the 1.4-ml cuvette at 10–20 μM, and at least 35 injections of 5 μl of the same buffer containing 15× concentrated Zn<sup>2+</sup> (150–300 μM) were made. Protein concentration was determined by both the Bradford assay and amino acid analysis. The data were analyzed using the MicroCal Origin program and best fitted to a one-site binding model.

**Limited Proteolysis**—The individual proteins were incubated with 1 mM DTT in 50 mM Tris, 150 mM NaCl (pH 7.4) at 4 °C overnight to reduce the proteins in the presence of 1 mM EDTA or 50 μM Zn<sup>2+</sup>. The reduced proteins with or without Zn<sup>2+</sup> as well as the oxidized proteins (untreated) then were incubated with trypsin in a ratio of 15:1 for a time as indicated and stopped by the addition of an excess of soybean trypsin inhibitor for 10 min at 4 °C. Samples were boiled at 95 °C and analyzed by Tris-Tricine SDS-PAGE followed by Coomassie Blue staining.

**Circular Dichroism Spectroscopy**—CD spectra were acquired using a JASCO J810 spectropolarimeter in 5 mM Tris (pH 7.6) at 25 °C using a 1-mm cuvette. A protein sample of 10 μM for Tim9 and/or Tim10 was used. Each spectrum represents an average of four scans from 260 to 190 nm at 0.2-nm intervals and the base line established by subtracting spectrum of the buffer. The signals are normalized by the total number of residues (87 for Tim9 and 93 for Tim10).

**Solution X-ray Scattering and Particle Shape Reconstruction**—Scattering data have been collected at station 2.1 of the SRS Daresbury Laboratory using a multi-wire gas detector and a sample-to-detector distance of 1.25 m that covered the momentum transfer interval 0.04 Å<sup>-1</sup> < *q* < 0.6 Å<sup>-1</sup>, where *q* = 4π sin θ/λ, 2θ is the scattering angle, and λ = 1.54 Å is the wavelength. The *q*-range was calibrated with the diffraction rings of silver behenate powder (based on a spacing of 58.38 Å). Samples were analyzed at 4 °C with protein concentrations in the range 0.5–7 mg/ml (Tim9 and Tim10) and 0.3–1 mg/ml (TIM10 complex). The total data collection time of 60 min (180 min) for the individual protein components (complex) provided sufficient statistics after averaging several independent measurements that were composed of 60-s time frames to check for radiation damage to the samples. Scattering profiles for the three protein samples (Tim9, Tim10, and complex) were analyzed using GNOM (22). The latter profile allows us to

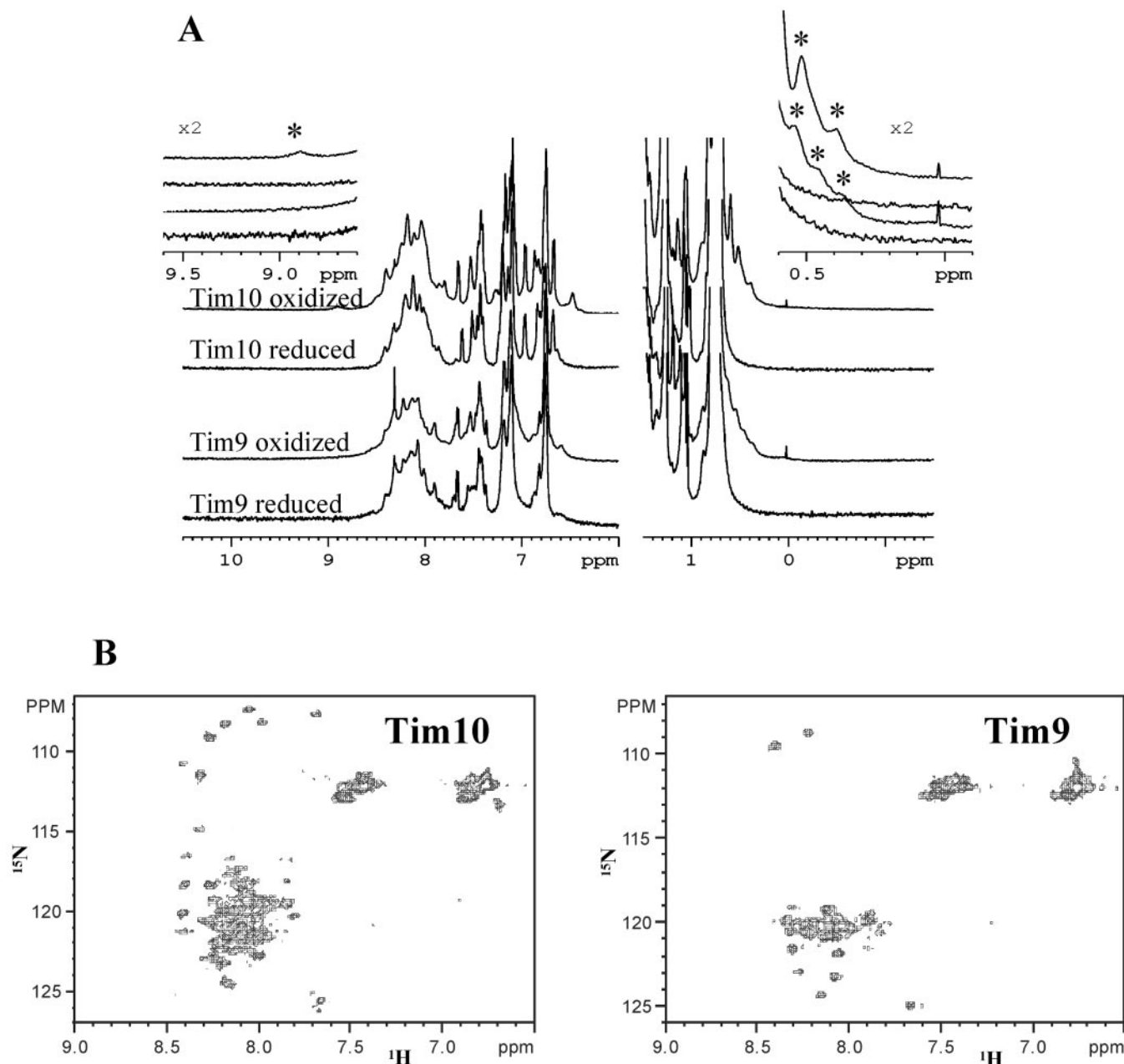


FIG. 1. Oxidized and reduced states of Tim9 and Tim10. *A*, one-dimensional  $^1\text{H}$  NMR spectra of individual Tim9 and Tim10 at the oxidized and reduced states without zinc. The *inset* shows a  $2\times$  blowout of the corresponding traces for better visualization. Asterisks indicate the new signals characteristic for the oxidized state. *B*, two-dimensional  $^1\text{H}$ - $^{15}\text{N}$ -HSQC spectra of oxidized Tim10 and Tim9 in free form.  $T = 293$  K.

evaluate structural parameters such as the radius of gyration ( $R_g$ ) and the maximum molecular dimension ( $D_{\text{max}}$ ) from the particle distance distribution function  $p(r)$  of a monodisperse protein solution, which represents the distributions of intramolecular distances between scattering centers within a protein molecule. Further details of data reduction and analysis are as published recently (23).

Particle shapes were restored from the experimental scattering profiles using the *ab initio* procedure based on the simulated annealing algorithm applied to a set of dummy spheres representing the amino acid chain of the molecules (24). Whereas the shape models for dimeric Tim9 and Tim10 have been calculated by means of 2-fold symmetry (with  $2 \times 87$  and  $2 \times 93$  amino acid residues, respectively), the molecular model for the complex was obtained by limiting the shape reconstruction to a 3-fold symmetry axis (using  $3 \times 180$  residues).

**Fluorescence Spectroscopy**—Fluorescence spectra of 8-anilino-1-naphthalenesulfonic acid (ANS, Sigma) were measured using a Varian Cary Eclipse fluorescence spectrophotometer. The TIM10 complex was used at a concentration of  $50 \mu\text{g/ml}$ , and ANS was used at 20 and  $50 \mu\text{M}$  in 50 mM Tris, 150 mM NaCl (pH 7.5). Fluorescence spectra were measured from 400 to 600 nm with an excitation wavelength set at 390

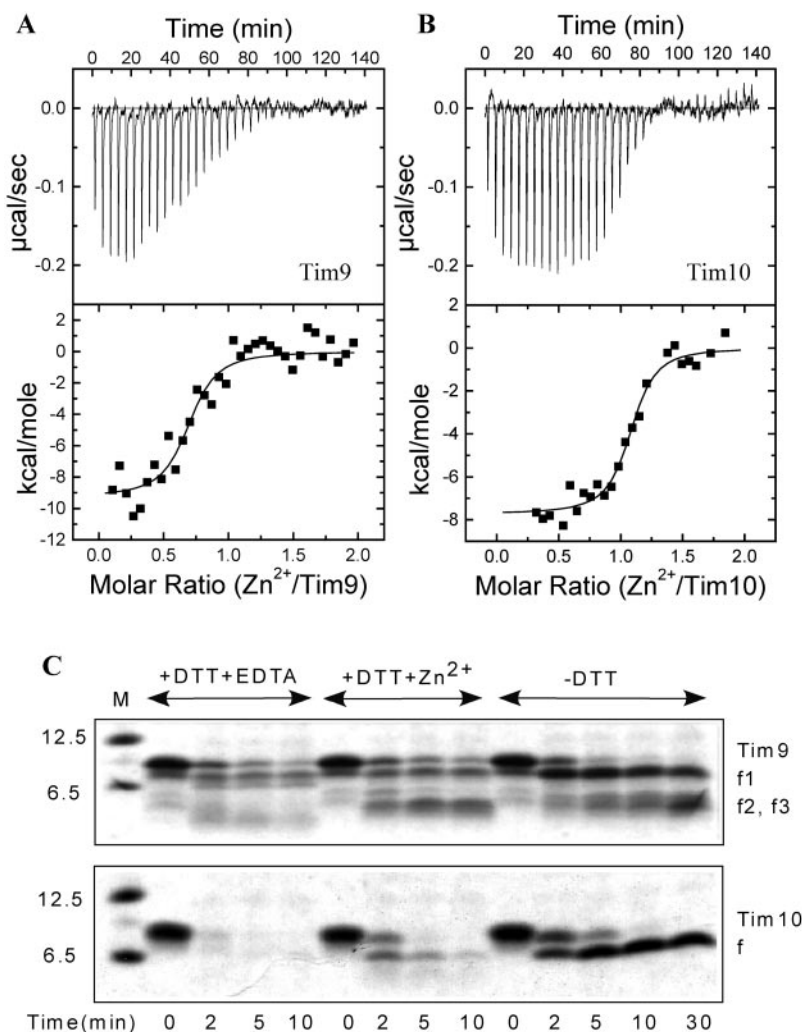
nm at  $25^\circ\text{C}$  using a  $2 \times 10$ -mm cuvette. A slit width of 5 nm was used for both excitation and emission.

## RESULTS

**Free Tim9 and Tim10 Are Partially Folded Molten Globules**—The global fold of the reduced and oxidized state of free (unassembled) Tim9 and Tim10 was studied by one-dimensional  $^1\text{H}$  NMR spectroscopy (Fig. 1*A*). From the increased linewidths and small chemical shift dispersion of the NMR signals, it is apparent that the reduced proteins exist as an ensemble of loosely folded interexchanging conformers. By contrast, oxidized Tim9 and Tim10 have greater chemical shift dispersion and thus more defined structures. New signals appear in the amide region between 8.5 and 9.0 ppm and in methyl region between 0.0 and 0.5 ppm (indicated by asterisk in Fig. 1*A*). The linewidths (as gauged from the resolved signals) are broader than expected for a protein of this size,

FIG. 2. Zinc binds and stabilizes the reduced Tim9 and reduced Tim10.

ITC measurements of the binding reaction of  $Zn^{2+}$  to the reduced Tim9 (panel A) and reduced Tim10 (panel B) in 10 mM metal-free HEPES buffer (pH 7.6) at 30 °C. Traces of the titration of 150  $\mu M$   $ZnCl_2$  into 10  $\mu M$  Tim9 or Tim10 in the cell are shown (top part). The integrated and normalized heats of injections for the binding (■) were fitted to a model describing one binding site (bottom plot, solid line). Analysis of the data yields a stoichiometry  $n = 0.7$  for  $Zn^{2+}/Tim9$  and 1 for  $Zn^{2+}/Tim10$  and a binding constant of  $K_a = 5 \times 10^5 M^{-1}$  and  $9 \times 10^6 M^{-1}$ , respectively. C, limited trypsinolysis of Tim9 and Tim10 at different states. +DTT+EDTA, reduced apoprotein; +DTT+ $Zn^{2+}$ , reduced protein with zinc; and -DTT, oxidized protein. The reaction was carried out at 4 °C by incubating the protein and trypsin at a ratio of 15:1 and stopped by the addition of 10 $\times$  mass excess of soybean trypsin inhibitor at the indicated times. Samples were analyzed by 16% Tris-Tricine SDS-PAGE followed by Coomassie Blue staining.



indicating that the native individual oxidized proteins most probably exist in a partially folded molten-globule state in which secondary structure elements (mainly  $\alpha$ -helices) are formed but which do not pack together in a unique way (Fig. 1A, compare *reduced versus oxidized* samples).

To gain further insight into the structure and dynamics of the individual oxidized proteins, the two-dimensional HSQC NMR spectra of  $^{15}N$ -labeled proteins were recorded (Fig. 1B). For both Tim9 and Tim10, two types of resonances are visible in the spectra, a set of sharp signals and a set of very broad signals, all of which have poor chemical shift dispersion. The sharp signals most probably originate from flexible unstructured regions of the molecules, which exhibit fast motions. The spectrum of Tim10 contains  $\sim 40$  such signals, seven of which have chemical shifts typical of glycines. In the spectrum of Tim9, approximately 22 intense signals were observed with at least two of these resonating at chemical shifts typical of glycine residues. Tim10 contains seven glycines, four of which are situated at the N terminus and three at the C terminus. Tim9 has four glycines at its C terminus. Broad signals in these spectra normally originate from regions of molecules that exist in molten-globule states. The presence of a mixture of sharp and broad resonances with many of the glycine signals being intense allow us to conclude that the most flexible and unstructured regions of Tim10 are probably located at both the N and C termini, whereas for Tim9 only the C terminus can be identified as unstructured. The middle regions of both proteins exist in molten-globule state, giving rise to broad signals. Many more sharp resonances are observed in the Tim10 spectrum,

suggesting that Tim10 has longer unstructured regions than Tim9. This is also borne out in the  $^{15}N$ -filtered one-dimensional spectra shown in Fig. 3, C and D. These NMR data provide a structural basis for the limited proteolysis on the individual proteins showing that the stable fragment f1 of Tim9 ( $\sim 8$  kDa) is larger than the fragment of Tim10 ( $\sim 6.5$  kDa) (Ref. 14 and Fig. 2C). Furthermore, N-terminal protein sequencing confirmed that fragment f1 of Tim9 starts from its N terminus and the fragment f of Tim10 starts from Ile<sup>18</sup>.

*Zinc Binds Only to the Reduced Tim9 and Tim10 and Is Coordinated by the Four Conserved Cys in the Repeated CX3C Motifs*—Zinc binding was studied using ITC at 30 °C. As shown in Fig. 2, A and B, there was a clear heat release when 15 $\times$  concentrated  $Zn^{2+}$  was injected into the reduced Tim9 or Tim10 where all of the thiols were reduced by 1 mM TCEP, showing that an exothermic binding reaction had occurred. In contrast, no heat change (hence no binding) was observed when zinc was injected into oxidized Tim9 or Tim10 (data not shown). The stoichiometry of zinc binding to the reduced Tim9 and reduced Tim10 was 0.7:1 and 1.1:1, respectively (Table I), suggesting a stoichiometry of one zinc ion per protein molecule. Zinc binding to only 70% of reduced Tim9 is presumably attributed to misfolding of some molecules. The binding constant was  $\sim 5 \times 10^6 M^{-1}$  and  $9 \times 10^6 M^{-1}$  for the proteins, respectively (Table I). The fact that the fully oxidized proteins did not bind zinc at all suggested that in the reduced state that the metal is coordinated by Cys residues of the “twin CX3C” motifs. We further confirmed this point by testing for metal binding to Tim10 mutants where each of the four conserved Cys was

TABLE I

Zinc binding properties of WT Tim9 and Tim10 and mutant Tim10 analyzed by ITC at 30 °C

NA, the parameters were not available because either zinc binding was too weak or the protein was not stable under the experimental conditions.

Protein	Ratio (Zn <sup>2+</sup> /protein)	Binding constant $K_d$ $M^{-1}$
WT Tim9	0.7	$5 \times 10^6 \pm 3 \times 10^6$
WT Tim10	1.1	$9 \times 10^6 \pm 3 \times 10^6$
C40S Tim10	NA	NA
C44S Tim10	1.4	$6 \times 10^5 \pm 3 \times 10^5$
C61S Tim10	NA	NA
C65S Tim10	0.4	$3 \times 10^4 \pm 2 \times 10^4$

exchanged for a Ser. As shown in Table I, Cys mutation resulted in clear defects in zinc binding, confirming that the metal is indeed coordinated by the Cys residues. The relatively low affinity is in agreement with the fact that both Tim9 and Tim10 are unable to retain zinc throughout the purification as measured by inductively coupled plasma-mass spectrometry (Peter Savory and Kostas Tokatlidis) (data not shown) (15).

**Zinc Binding Stabilizes the Reduced State**—To test for the stability of the three different structural states of free Tim9 and Tim10, *i.e.* the reduced state with and without zinc and the oxidized state, we performed limited trypsinolysis as shown in Fig. 2C. The oxidized states are mostly stable, especially the fragments corresponding to the stable core delineated by the two CX3C motifs. The reduced proteins that were unfolded by DTT are readily cleaved, but in the presence of zinc, they become more protease-resistant. We conclude that zinc binding stabilizes the reduced Tim9 and Tim10 against proteolysis. In contrast, Tim10 Cys mutants that cannot bind zinc as tightly as the wild type protein remain largely protease-sensitive in their reduced state (data not shown). Far-UV CD spectra of the reduced proteins before and after zinc binding showed no detectable secondary structure change upon zinc binding (data not shown). This is in agreement with the fact that zinc ligation often does not impose any extra constraints on secondary structure as can be deduced by an analysis of zinc binding sites in several crystal structures of zinc-binding proteins.

**Distinct Structural Changes of Tim9 and Tim10 upon TIM10 Complex Formation**—CD and NMR spectroscopy were used to elucidate the conformational changes associated with the assembly process. When comparing the CD spectrum of the complex (Fig. 3A, *black line*) to the one produced by adding up the spectra of the individual proteins under identical conditions (Fig. 3A, *gray line*), a clear difference could be seen in the spectra above and below 208 nm and in particular at the characteristic minimum of 222 nm for  $\alpha$ -helix, indicating a structural change upon complex formation.

Global three-dimensional structural changes were then examined by <sup>1</sup>H NMR. As a control, the mixing of reduced Tim9 and Tim10 in a 1:1 ratio did not show any associated changes in chemical shifts (Figs. 1A and 3B); however, mixing oxidized proteins produced a spectrum that is quite different from the simple sum of the individual oxidized Tim9 and Tim10 spectra. New signals appear in the spectrum of the complex in the methyl region (0.0–0.5 ppm) and amide region (8.5–9.5 ppm). The linewidths are sharper than for individual oxidized proteins, and they are consistent with the molecular mass of the complex (70 kDa). These results show that global changes of the three-dimensional structure rather than simple localized changes are concomitant with complex formation. To monitor the subunit-specific structural changes attributed to complex formation, we observed the changes in <sup>15</sup>N-filtered one-dimensional NMR spectra when non-labeled counterpart has been

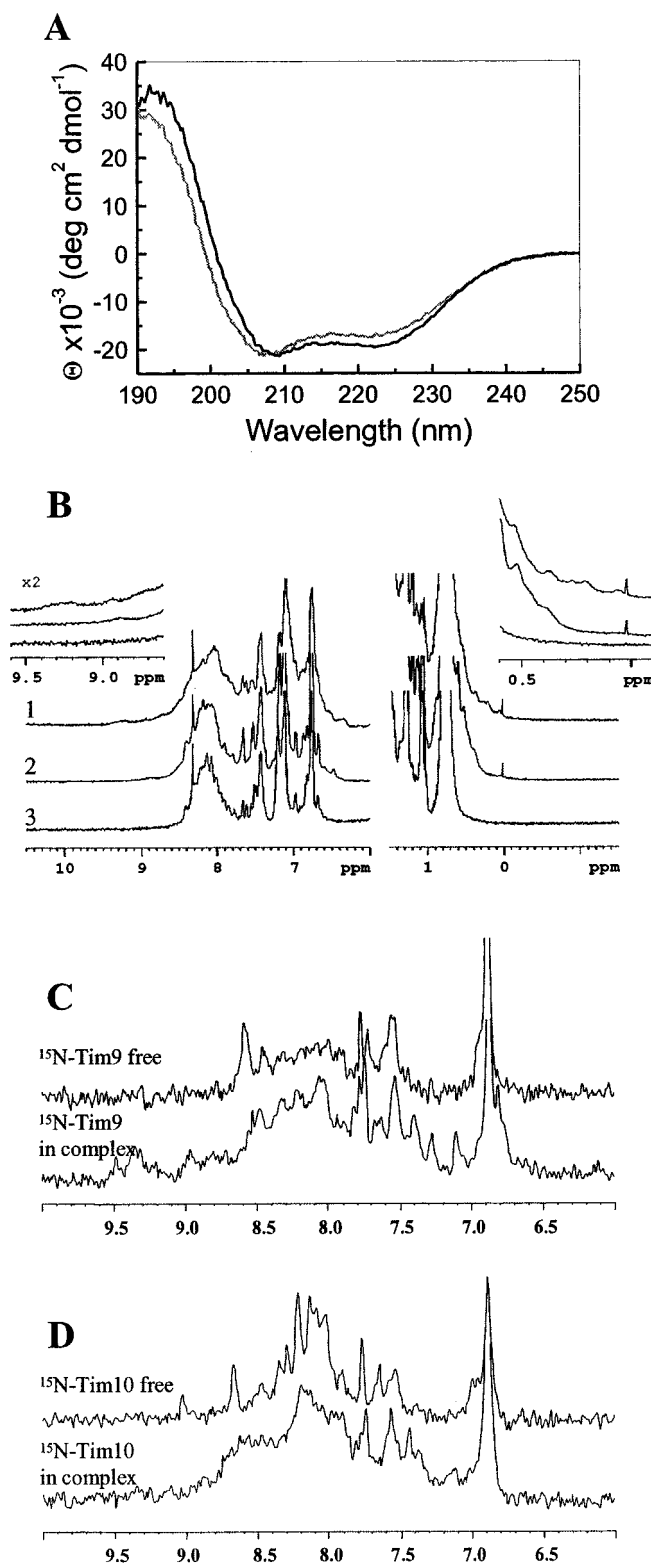


FIG. 3. Structural changes underpinning TIM10 complex formation. A, far-UV CD spectra of the purified TIM10 complex in 5 mM Tris buffer (pH 7.4) (*black line*) compared with the calculated spectra of Tim9 plus Tim10 (*gray line*). B, one-dimensional <sup>1</sup>H NMR spectra of complex between oxidized Tim9 and Tim10 (*trace 1*) compared with the sum of spectra of the individual oxidized subunits (*trace 2*) and 1:1 mixture of reduced Tim9 and Tim10 (*trace 3*). The inset represents a 2× blowout of the respective graph for better visualization. C, one-dimensional <sup>15</sup>N-filtered <sup>1</sup>H NMR spectra of oxidized <sup>15</sup>N-labeled Tim 9 in the free form (*top*) and when complexed to non-labeled Tim 10 (*bottom*). D, one-dimensional <sup>15</sup>N-filtered <sup>1</sup>H NMR spectra of oxidized <sup>15</sup>N-labeled Tim10 in the free form (*top*) and when complexed to non-labeled Tim9 (*bottom*).

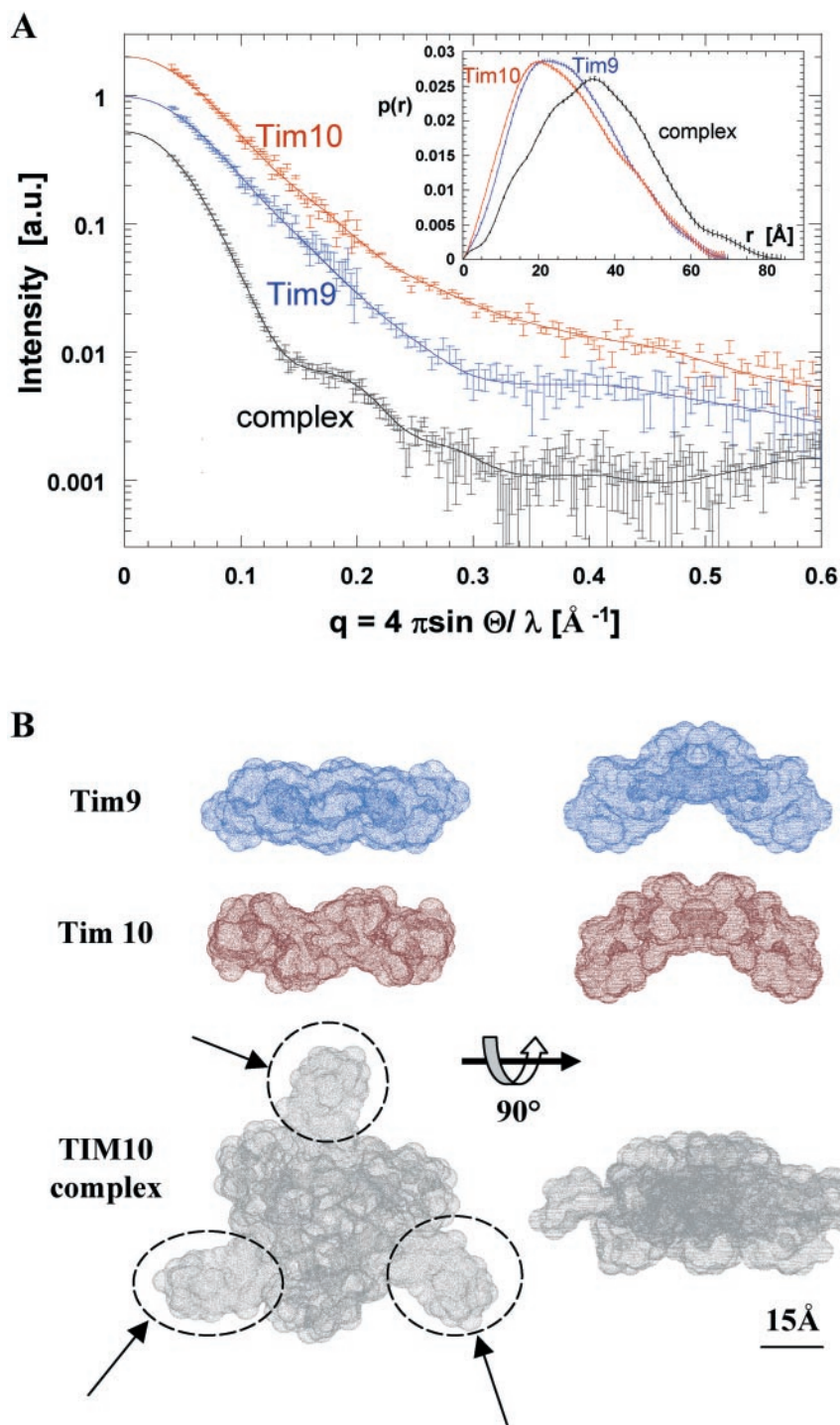


FIG. 4. **Solution x-ray scattering data and the deduced low resolution structures of Tim9, Tim10, and their complex TIM10.** *A*, scattering data (dots with error bars) and curves from the restored models (full lines shown in *B*) of individual oxidized Tim9, Tim10 (in dimeric form), and the hetero-hexameric TIM10 complex. For better visualization, curves have been displaced. The inset shows the  $p(r)$  functions (normalized to unit area). *B*, three-dimensional models restored from the solution x-ray scattering data presented in *A*. The flexible protruberances in the complex (see “Results”) are circled in dotted line and indicated by arrows. The right views are rotated clockwise by  $90^\circ$  around the horizontal axis as indicated. For Tim9/Tim10, the following structural parameters were deduced, respectively:  $R_g = 22.3 \pm 0.2 \text{ \AA} / 21.9 \pm 0.2 \text{ \AA}$ ;  $D_{\max} = 71 \pm 2 \text{ \AA} / 68 \pm 2 \text{ \AA}$ ; and  $V = 44,000 \pm 3000 \text{ \AA}^3 / 3200 \pm 2600 \text{ \AA}^3$ . For the assembled TIM10 complex,  $R_g = 27.7 \pm 0.2 \text{ \AA}$ ;  $D_{\max} = 85 \pm 3 \text{ \AA}$ ; and  $V = 99,000 \pm 5000 \text{ \AA}^3$ .

added to either  $^{15}\text{N}$ -labeled Tim9 or Tim10. Fig. 3, *C* and *D*, show the results of experiments where  $^{15}\text{N}$ -labeled Tim9 interacted with unlabeled Tim10 and *vice versa*. Although both Tim9 and Tim10 demonstrate significant changes in spectra upon complex formation, the two proteins behave differently. The spectrum of Tim9 in complex has significantly better chemical shift dispersion than that of Tim10. The new signals appearing in the amide region between 8.5 and 9.5 ppm originating from complexed Tim9 show characteristics of a protein with defined structure with large dispersion of chemical shifts and linewidths consistent with the expected molecular mass of the complex (70 kDa). Unlike Tim9, the spectrum of Tim10 in complex has poor chemical shift dispersion with characteristics of molten-globule state. The differences in changes in their

respective dynamics upon complex formation between Tim9 and Tim10 may reflect the fact that these two components of TIM10 play different roles in chaperone assembly and function.

*The Novel Three-dimensional Structure of the TIM10 Complex and of the Individual Tim9 and Tim10 Determined by SAXS*—Because nothing is known regarding the three-dimensional structures of any of the “small Tim” family or their complex, it was of great interest to determine these structures for Tim9 and Tim10. X-ray crystallography is the obvious method to determine the structure to atomic resolution, but this has not been successful so far for this complex, probably because of the flexibility of the proteins. NMR, on the other hand, would be an alternative, and work is underway to obtain high resolution information. Electron microscopy has been

used to obtain low resolution structures for the TIM22 and TOM40 complexes (25–28), but the size of the TIM10 complex (70 kDa) is rather small, hindering the application of this method. Therefore, we obtained the low resolution three-dimensional structure of the individual proteins and their complex from SAXS experiments (Fig. 4). Molecular structures were restored from scattering data (24) that was collected up to a Bragg resolution of 10 Å. The method considers the protein structure as an assembly of dummy residues centered at the  $C_{\alpha}$  positions. Subsequently, a molecular envelope is constructed by finding a chain-compatible spatial arrangement that fits the experimental scattering data. This method has been used successfully for many proteins (23, 29) with the advantage of analysis of native particles in nearly physiological conditions. The SAXS structures of individual dimers Tim9 and Tim10 are broadly similar with some subtle but detectable differences. (i) Tim9 has a slightly less compact shape and is more elongated than Tim10 (Tim9 appears to make use of a bigger molecular volume), in agreement with previous analytical ultracentrifugation data (14). (ii) When the particles were turned 90°, the cleft in Tim10 is shown to be larger than Tim9. (iii) At the top part of the particles, Tim9 has a distinct protuberance toward the solvent whereas Tim10 has a minor cleft (Fig. 4, *A* and *B*). The TIM10 complex particle was reconstructed based on a 3-fold symmetry, in agreement with its stoichiometry of three Tim9 to three Tim10 experimentally determined by MS and ITC (14, 15). Comparing the individual proteins to the holo-complex, it is apparent that merely based on size considerations a structural rearrangement has to occur during complexation. There is a central core with higher density and two classes of protuberances pointing outside. Three are quite large, whereas the other three are significantly shorter and near the core of the complex. Several shape reconstructions indicate that the large protuberances (shown by *arrows*) can move significantly and are therefore rather flexible. As we used a 2–3-fold symmetry for the individual proteins and the complex respectively, the number of possible solutions to the problem of uniqueness of shapes is drastically reduced. Furthermore, rerunning shape reconstructions in several independent experiments comes up with very similar shapes and shows that the envelope we present can be considered as a representative shape model. Together with the NMR data, we suggest that the large flexible protuberances may well represent Tim10 in the complex. We would speculate that the protuberances and clefts represent functionally important domains for the interaction with the substrate ADP/ATP carrier that also has an internal 3-fold symmetry (30) and/or subunits of the TIM22 complex. The overall size of the particle is rather large ( $D_{\max} = 85 \pm 3$  Å), which would allow it to span most of the intermembrane space (average distance 140 Å measured for mammalian mitochondria) (31), thus providing an extended chaperone scaffold surface for the hydrophobic substrates. In contrast to most other known chaperones, TIM10 does not have a doughnut-shaped structure or any extensive internal cavities into which the unfolded substrate could fit. This unique structure may reflect the fact that this is not an ATP-powered chaperone with substrate binding and release relying on conformational changes induced by the substrate itself and/or other components of the insertion pathway. Scanning the Protein Data Bank for similar-sized symmetrical particles, calculating their theoretical scattering profiles and comparing them to the experimental data of the TIM10 particle did not yield convincing fits, indicating that this structure is novel.

*The TIM10 Complex Has Increased Surface Hydrophobicity*—Given that TIM10 binds the hydrophobic carriers in transit and no atomic resolution data are available to define specific substrate

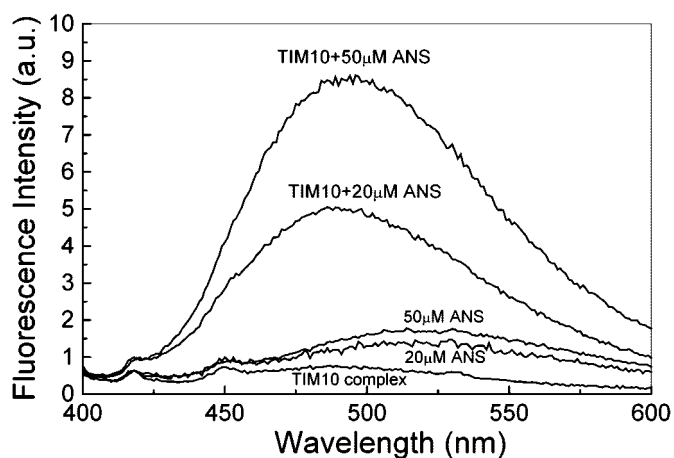


FIG. 5. Fluorescence emission spectra of ANS in the presence or absence of 50  $\mu\text{g/ml}$  TIM10 complex indicates that this complex has increased surface hydrophobicity.

binding clefts, we examined experimentally the surface hydrophobicity of the complex by monitoring changes in the intrinsic ANS fluorescence (Fig. 5) on binding TIM10. A significant concentration-dependent increase in ANS fluorescence was observed, indicating the binding of hydrophobic segments of the TIM10 complex to ANS. Such a behavior is often observed for the molten-globule state of several proteins (32) and would be consistent with the molten-globule characteristics of TIM10 as shown above by NMR. The hydrophobic interaction between TIM10 and ANS could be emulating similar interactions between the complex and hydrophobic substrates.

#### DISCUSSION

The data presented here are the first direct evidence of the structure of the Tim9 and Tim10 proteins and their complex under a variety of conditions. Also, these experimental data provide a structural basis to a model for the redox-regulated multi-step mechanism of biogenesis and assembly of the TIM10 complex that we first postulated based on a combination of site-directed mutagenesis and functional studies (19, 44). The major stages in this pathway are as follows: stage 1, the individual subunits Tim9 and Tim10 are maintained in an unfolded structure in the cytosol; and stage 2, the subunits are imported in a reduced state, which is assembly-incompetent. Either stage 1 or 2 may be stabilized by zinc, which would have to be added to the apoprotein by a specific zinc-dependent chaperone, because the intrinsic affinity of the proteins for zinc is very low. Potential metal binding at this stage would have a clear stabilizing effect but does not significantly increase secondary structure content. In stage 3, the unassembled subunits are folded to a molten-globule state that is maintained structurally by oxidation of the four cysteines into two intrachain disulfides. This is an assembly-competent state. Tim9 is more folded than Tim10, which maintains extensive flexibility particularly of its N and C termini in this state. In stage 4, the two oxidized subunits associate in a 3:3 stoichiometry to form the stable, fully functional TIM10 particle with the three-dimensional structure shown in Fig. 4. This model does not invoke the direct requirement of zinc for the assembly process.

The fact that the proteins have to be in a reduced, hence, unfolded state to get imported is not entirely surprising based on the generally accepted idea that tightly folded domains inhibit transport to mitochondria. However, one could still argue that, for Tim10, the oxidized state could be imported based on two considerations. (i) The small size (11 Å) of the monomeric oxidized Tim10 would allow passage through the Tom40 pores of  $\sim 22$  Å (26–28, 33, 34). (ii) The oxidized state is

not tightly folded but rather adopts a molten-globule conformation that has been previously suggested to be a translocation-competent conformation (35, 36). However, Tim10 must be fully reduced for it to be imported. This indicates that the outer membrane protein import channel clearly cannot accommodate the molten-globule state for Tim10. These data extend the studies of Matouschek and colleagues (37, 38), showing that presequence-containing precursors targeted to the matrix must be significantly unfolded during import. Although Tim10 differs from these precursors in that (i) it is an authentic mitochondrial protein, (ii) its structure is mainly  $\alpha$ -helical, (iii) it does not carry a presequence, and (iv) it is transported only through the outer membrane channel independently of the function of the mHsp70 translocation motor and the inner membrane electrochemical potential, it appears to be obeying the same strict requirement for complete absence of disulfides in its structure as presequence-containing precursors.

The intrinsic flexibilities of Tim9 and Tim10 together with their tendency to aggregate make the high resolution structure determination by either x-ray crystallography or NMR challenging. Hence, we present the low resolution three-dimensional structure of the complex obtained from SAXS, a method that is capable of providing structural resolution equivalent to electromagnetic studies but which is more suitable for particles the size of the TIM10 complex. The SAXS structure of the TIM10 complex shows some striking novel features. The restored model supports its biological role as a chaperone, providing a potential to span a significant part of the space between the outer and inner membranes, hence "shielding" the hydrophobic substrate and preventing aggregation. Based on the different structural properties of the two subunits within the complex, it is tempting to speculate that the more mobile parts of the structure can be assigned to Tim10 and that these reflect specific functional roles as well. The overall flexibility of the TIM10 structure revealed from both NMR and SAXS data has several important functional consequences. The intrinsically low degree of ordered structure for these proteins explains why they can bind to a large array of substrates (10) with relative low affinity (3), thus ensuring binding efficiency (2, 3). This is of central importance to their function because they not only have to bind an incoming precursor but also release it to the insertion-specific TIM22 complex. In more general terms, it has been suggested that an increasing number of proteins are intrinsically disordered or retain very flexible conformations for most of their lifetime in the cell (39–41). Many of those are involved in cell signaling and regulation (42), and flexibility is thought to allow them to cope better with changes and bind to several different targets (42, 43). Tim9 and Tim10 set an example of such proteins where flexibility rather than a tightly folded structure facilitates their substrate recognition and translocase function in mitochondria.

**Acknowledgments**—We thank Neil Bulleid, Tassos Economou, Dave Thornton, and members of our laboratory for discussions and comments on the paper. SAXS data were collected at Daresbury Laboratory (Beamtime Grants 38/265 and 39/091).

#### REFERENCES

- Pfanner, N., and Geissler, A. (2001) *Nat. Rev. Mol. Cell. Biol.* **2**, 339–349
- Koehler, C. M., Merchant, S., and Schatz, G. (1999) *Trends Biochem. Sci.* **24**, 428–432
- Tokatlidis, K., and Schatz, G. (1999) *J. Biol. Chem.* **274**, 35285–35288
- Chacinska, A., Pfanner, N., and Meisinger, C. (2002) *Trends Cell Biol.* **12**, 299–303
- Bauer, M. F., Hofman, S., Brunner, M., and Neupert, W. (2000) *Trends Cell Biol.* **10**, 25–31
- Koehler, C. M., Merchant, S., Oppliger, W., Schmid, K., Jarosch, E., Dolfini, L., Junne, T., Schatz, G., and Tokatlidis, K. (1998) *EMBO J.* **17**, 6477–6486
- Sirrenberg, C., Endres, M., Folsch, H., Stuart, R. A., Neupert, W., and Brunner, M. (1998) *Nature* **391**, 912–915
- Koehler, C. M., Jarosch, E., Tokatlidis, K., Schmid, K., Scheweyen, R. J., and Schatz, G. (1998) *Science* **279**, 369–373
- Adam, A., Endres, M., Sirrenberg, C., Lottspeich, F., Neupert, W., and Brunner, M. (1999) *EMBO J.* **18**, 313–319
- Leuenerberger, D., Bally, N. A., Schatz, G., and Koehler, C. M. (1999) *EMBO J.* **18**, 4816–4822
- Davis, A. J., Sepuri, N. B., Holder, J., Johnson, A. E., and Jensen, R. E. (2000) *J. Cell Biol.* **150**, 1271–1282
- Paschen S. A., Rothbauer, U., Kaldi, K., Bauer, M. F., Neupert, W., and Brunner, M. (2000) *EMBO J.* **19**, 6392–6400
- Sirrenberg, C., Bauer, M. F., Guiard, B., Neupert, W., and Brunner, M. (1996) *Nature* **384**, 582–585
- Vial, S., Lu, H., Allen, S., Savory, P., Thornton, D., Sheehan, J., and Tokatlidis, K. (2002) *J. Biol. Chem.* **277**, 36100–36108
- Curran, S. P., Leuenerberger, D., Oppliger, W., and Koehler, C. M. (2002) *EMBO J.* **21**, 942–953
- Truscott, K. N., Wiedemann, N., Rehling, P., Muller, H., Meisinger, C., Pfanner, N., and Guiard, B. (2002) *Mol. Cell. Biol.* **22**, 7780–7789
- Luciano, P., Vial, S., Vergnolle, M. A., Dyall, S. D., Robinson, D. R., and Tokatlidis, K. (2001) *EMBO J.* **20**, 4099–4106
- Lutz, T., Neupert, W., and Herrmann, J. M. (2003) *EMBO J.* **22**, 4400–4408
- Allen, S., Lu, H., Thornton, D., and Tokatlidis, K. (2003) *J. Biol. Chem.*, **278**, 38505–38513
- Hoffmann, S., Rothbauer, U., Muhlenbein, N., Neupert, W., Gerbitz, K. D., Brunner, M., and Bauer, M. F. (2002) *J. Biol. Chem.* **277**, 23287–23293
- Roesch, K., Curran, S. P., Tranejbaerg, L., and Koehler, C. M. (2002) *Hum. Mol. Genet.* **11**, 477–486
- Semenyuk, A. V., and Svergun, D. I. (1991) *J. Appl. Crystallogr.* **24**, 537–540
- Witty, M., Sanz, C., Shah, A., Grossmann, J. G., Mizuguchi, K., Perham, R. N., and Luisi, B. (2002) *EMBO J.* **21**, 4207–4218
- Svergun, D. I., Petoukhov, M. V., and Koch, M. H. (2001) *Biophys. J.* **80**, 2946–2953
- Rehling, P., Model, K., Brandner, K., Kovermann, P., Sickmann, A., Meyer, H. E., Kuhlbrandt, W., Wagner, R., Truscott, K. N., and Pfanner, N. (2003) *Science* **299**, 1747–1751
- Ahting, U., Thun, C., Hegerl, R., Typke, D., Nargang, F. E., Neupert, W., and Nussberger, S. (1999) *J. Cell Biol.* **147**, 959–968
- Kunkele, K. P., Heins, S., Dembowski, M., Nargang, F. E., Benz, R., Thieffry, M., Walz, J., Lill, R., Nussberger, S., and Neupert, W. (1998) *Cell* **93**, 1009–1019
- Model, K., Prinz, T., Ruiz, T., Radermacher, M., Krimmer, T., Kuhlbrandt, W., Pfanner, N., and Meisinger, C. (2002) *J. Mol. Biol.* **316**, 657–666
- Grossmann, J. G., Sharff, A. J., O'Hare, P., and Luisi, B. (2001) *Biochemistry* **40**, 6267–6274
- Saraste, M., and Walker, J. E. (1982) *FEBS Lett.* **144**, 250–254
- Frey, T. G., and Mannella, C. A. (2000) *Trends Biochem. Sci.* **25**, 319–324
- Uversky, V. N., Winter, S., and Lober, G. (1996) *Biophys. Chem.* **60**, 79–88
- Hill, K., Model, K., Ryan, M., Dietmeier, K., Martin, F., Wagner, R., and Pfanner, N. (1998) *Nature* **395**, 516–521
- Schwartz, M. P., and Matouschek, A. (1999) *Proc. Natl. Acad. Sci. U. S. A.*, **96**, 13086–13090
- Ptitsyn, O. B. (1995) *Adv. Protein Chem.* **47**, 83–229
- van der Goot, F. G., Lakey, J. H., and Pattus, F. (1992) *Trends Cell Biol.* **2**, 343–348
- Huang, S., Ratliff, K. S., Schwartz, M. P., Spenner, J. M., and Matouschek, A. (1999) *Nat. Struct. Biol.* **6**, 1132–1138
- Schwartz, M. P., Huang, S., and Matouschek, A. (1999) *J. Biol. Chem.* **274**, 12759–12764
- Kriwacki, R. W., Hengst, L., Tennant, L., Reed, S. I., and Wright, P. E. (1996) *Proc. Natl. Acad. Sci. U. S. A.*, **93**, 11504–11509
- Wright, P. E., and Dyson, H. J. (1999) *J. Mol. Biol.* **293**, 321–331
- Golovanov, A. P., Chuang, T. H., DerMardirossian, C., Barsukov, I. L., Hawkins, D., Badii, R., Bokoch, G. M., Lian, L.-Y., and Roberts, G. C. K. (2001) *J. Mol. Biol.* **305**, 121–135
- Dunker, A. K., and Obradovic, Z. (2001) *Nat. Biotechnol.* **19**, 805–806
- Shoemaker, B. A., Portman, J. J., and Wolynes, P. G. (2000) *Proc. Natl. Acad. Sci. U. S. A.* **97**, 8868–8873
- Lu, H., Allen, S., Wardleworth, L., Savory, P., and Tokatlidis, K. (2004) *J. Biol. Chem.* **279**, 18952–18958